Catalysis Science & Technology

Accepted Manuscript

ROYAL SOCIETY OF CHEMISTRY

www.rsc.org/catalysis

Graphical Abstract:

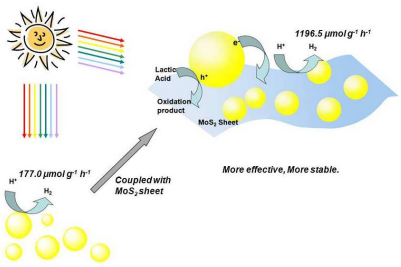

A novel nanocomposite composed of graphene-like MoS_2 sheet and $Zn_xCd_{1-x}S$ nanoparticles was used for photocatalytic hydrogen under visible light.

Cite this: DOI: 10.1039/c0xx00000x

www.rsc.org/xxxxxx

ARTICLE TYPE

Coupling $Zn_xCd_{1-x}S$ nanoparticles with graphene-like MoS_2: superior interfacial contact, low overpotential and enhanced photocatalytic activity under visible-light irradiation

Yongtao Lu,[a] Dandan Wang,[a] Ping Yang,[a*] Yukou Du,[a] and Cheng Lu[b*a]

Received (in XXX, XXX) Xth XXXXXXXXX 20XX, Accepted Xth XXXXXXXXX 20XX
DOI: 10.1039/b000000x

Abstract: A novel nanocomposite composed of two-dimensional graphene-like MoS_2 and $Zn_xCd_{1-x}S$ ($0 \le x \le 0.5$) nanoparticles has been synthesized by a simple exfoliation of bulk MoS_2 into single- or few-layer MoS_2 and then ultrasonic mixing $Zn_xCd_{1-x}S$ onto MoS_2 nanosheets. The samples were characterized by X-ray diffraction (XRD), X-ray photoelectron spectroscopy (XPS), high-resolution transmission electron microscopy (HRTEM), UV-visible diffuse reflectance spectroscopy (UV-vis DRS), photoelectrochemical experiment and photoluminescence. The results showed that the nanoparticles of $Zn_xCd_{1-x}S$ were well dispersed and anchored on the surface of the graphene-like MoS_2 nanosheets. The superior interfacial coupling between $Zn_xCd_{1-x}S$ and MoS_2 synergistically promoted the electron-holes transportation and separation. Upon visible-light irradiation (λ>420 nm), the composite consisted of $Zn_{0.3}Cd_{0.7}S$ and ca. 0.6 wt% graphene-like MoS_2 gives the highest hydrogen evolution amount of 7179.1 μmol g^{-1}, which is ca. 7 times as high as that of $Zn_{0.3}Cd_{0.7}S$. This study displays a facile method to build a low-cost but effective photocatalyst for water reduction to produce hydrogen under solar light irradiation.

* [a] College of Chemistry, Chemical Engineering and Materials Science, Soochow University, Suzhou 215123, China. E-mail: pyang@suda.edu.cn; Fax: +86-512-6588 0089; Tel: +86-512-6588 0089; [b] Department of Chemistry and Physics, University of Toronto, Toronto M5S 3H6, Canada Tel/Fax: 1-416-978-4526; Email: clu@chem.utoronto.ca.

Cite this: DOI: 10.1039/c0xx00000x

www.rsc.org/xxxxxx

ARTICLE TYPE

1. Introduction

Due to the global energy crisis and environmental protection demand, hydrogen as an environmentally friendly and recyclable energy has attracted great attention. The photocatalytic water splitting to produce hydrogen has been considered as one of the most important technologies to solve the energy crisis and environmental issues.[1-3] Since Fujishima and Honda reported H_2 evolution from TiO_2 electrode,[4] many novel semiconductor-based photocatalytic hydrogen generation systems, including CdS,[5-9] C_3N_4,[10-14] TaON,[15-16] etc. have been developed. Various technologies such as forming solid solutions,[17-19] semiconductor combination,[20-23] co-catalyst loading,[5-7,9,24] sensitization with organic dyes,[25-26] and morphology controlling,[27-28] have been adopted to improve the catalytic performance of the photocatalysts. For example, Wong's group combined zinc cadmium sulphide with MoS_2 using an in-situ photo-assisted deposition method. This novel composite photocatalyst showed enhanced photocatalytic activity for hydrogen evolution compared to sole zinc cadmium sulphide.[29] Among the investigated semiconductors, CdS has excellent visible-light absorption ability with a sufficient narrow band gap (Eg ~ 2.4 eV). However, CdS without cocatalyst usually is low active for the photocatalytic hydrogen production from water because of its large H_2 evolution overpotential. Another most investigated semiconductor ZnS is found to be an effective photocatalyst for H_2 evolution even in the absence of noble metal co-catalysts since it has high conduction band potential.[30-32] Unfortunately, ZnS is a wide band gap semiconductor (3.5 eV) and can only be active for H_2 evolution under UV-light irradiation. Reber's group first demonstrated that forming $Zn_xCd_{1-x}S$ solid solution between ZnS and CdS improved the photoactivity obviously.[5] After this work, the $Zn_xCd_{1-x}S$ solid solution prepared in different method as a photocatalyst for water splitting in visible-light region has been investigated intensively.[17-18, 33-35] The results demonstrated that though $Zn_xCd_{1-x}S$ might be used as a visible-light active photocatalyst for reduction of water to produce hydrogen in the presence of sacrificial electron donors, the quantum efficiency was still relatively low. The hybridization of semiconductors with other materials to facilitate charge transfer and separation has been proved to be another powerful strategy to improve the photocatalytic activity.[20-23] Various effective methods, including coupling the semiconductors with graphene or carbon tubes, have been developed. Coupling a semiconductor with graphene produces a kind of novel photocatalysts for hydrogen production since graphene can accommodate the photogenerated charges transfer and suppress charges recombination.[36-38] Inspired by the outstanding properties of graphene, some graphene-like materials like molybdenum disulfide (MoS_2), have also attracted considerable attention. MoS_2 with a layered structure consisting of sulfur layers with Mo ions in between can be exfoliated to single- or few-layer nanosheets similarly as what observed in graphene.[39] It has also been reported that MoS_2 demonstrated low overpotential for hydrogen evolution reaction.[40] With these outstanding properties, graphene-like MoS_2 sheet can act as an excellent supporting matrix and a non-noble metal co-catalyst.

Herein, we report the fabrication, characterization and photocatalysis of a novel nanocomposite composed of two-dimensional graphene-like MoS_2 and $Zn_xCd_{1-x}S$ ($0 \le x \le 0.5$) solid solution. The nanocomposite was prepared by a simple exfoliation of bulk molybdenum disulfide into single- or few-layer MoS_2 and then ultrasonic mixing $Zn_xCd_{1-x}S$ onto graphene-like MoS_2 nanosheets. The as-prepared nanocomposite demonstrates a high photocatalytic activity for H_2 evolution under visible-light irradiation without adding the noble-metal co-catalyst. The enhancement of photocatalytic activity may be attributed to the superior interfacial contacts between $Zn_xCd_{1-x}S$ and two-dimensional MoS_2 nanosheets, which could synergistically promote the electron-holes transportation and separation. The structure, optical and photoelectrochemical properties of the composite have been fully investigated. Our work demonstrated a new prototype for constructing a low-cost but effective photocatalyst for water reduction to produce hydrogen under solar light irradiation.

2. Experimental

2.1. Materials and Syntheses

All chemicals were purchased from Sinopharm chemical reagent company and used without further purification.

The $Zn_xCd_{1-x}S$ was synthesized by a hydrothermal treatment. In a typical experiment, zinc acetate ($Zn(Ac)_2 \cdot 2H_2O$) and cadmium sulfate ($3CdSO_4 \cdot 8H_2O$) in a total amount of 6 mmol with various molar ratios were dissolved in 40 mL of deionized water, then 20 mL of 0.45 M sodium sulfide ($Na_2S \cdot 9H_2O$) solution was added dropwise under magnetic stirring. The mixture was transferred to a 100 mL Teflon-lined autoclave and heated at 180 °C for 10 h. The solid was isolated by centrifugation, washed with deionized water for 3 times and dried at 70 °C. The resultant samples were stored in the darkness before further dealing with.

MoS_2 was prepared following the reported method with some modifications.[41-42] To a 100 mL Teflon-lined autoclave, 1.45 g (6 mmol) of $Na_2MoO_4 \cdot 2H_2O$, 2.28 g (30 mmol) of thiourea and 60 mL of deionized water were added. The autoclave with the reactants was heated to 210 °C and kept at the temperature for 24 h. The autoclave was cooled to room temperature and the black precipitate was collected by centrifugation. The resulting solid was washed with deionized water for 3 times, and then dried in an oven at 70 °C for 24 h. Single- or few-layered graphene-like MoS_2 was prepared by exfoliation of MoS_2 in an organic solvent.[39,43] In a typical experiment, 750 mg of MoS_2 was dispersed in 15 mL of methanol in a 100 mL flask. The mixture was sonicated for 2 h at room temperature, resulting in a dark brown suspension. The suspension was centrifuged for 10 min

(2000 rpm) and the residue was removed by decantation. The concentration of as-prepared single- or few-layered graphene-like MoS_2 in the suspension was ca. 0.6 mg mL^{-1}.

$Zn_xCd_{1-x}S$ functionalized graphene-like MoS_2 was prepared by an ultrasonic mixing method. An appropriate amount of the $Zn_xCd_{1-x}S$ sample was added in 50 mL of MoS_2 suspension (containing ca. 2 mg MoS_2) and the mixture was ultrasonicated for another 2 hours. After that, the solvent was removed on a rotary evaporator at 40 °C. The obtained lamellar solid was grinded into powders. The as-prepared sample labeled as $Zn_xCd_{1-x}S/MoS_2$-y, where y stands for weight percent of MoS_2 in the nanocomposite. All samples were stored in the darkness before used for the photocatalytic reactions.

2.2. Characterization

Powder X-ray diffraction (XRD) patterns were recorded on an X-ray diffractometer (X' Pert-ProMPD) with Cu Kα irradiation (λ=1.5406 Å). X-ray photoelectron spectroscopy (XPS) was performed on the Thermo Scientific ESCALA 250Xi X-ray Photoelectron Spectrometer. All the binding energies were calibrated by C 1s peak at 284.5 eV of the surface adventitious carbon. Transmission electron microscopy (TEM) studies were conducted on a transmission electron microscope (JEOL JEM-2100) operating at an accelerating voltage of 200 kV. The ultraviolet-visible diffuse reflectance spectra (DRS) were obtained on a UV-visible spectrophotometer (Shimadzu UV-3150). Photoluminescence (PL) spectra of the samples were recorded on an Edinburgh PLS920 fluorospectrophotometer.

2.3. Photoelectrochemical measurement

The photoelectrochemical behaviors of the samples were measured on a CHI660D potentiostat/galvanostat electrochemical analyzer in a three-electrode system consisting of a working electrode, a platinum wire as a counter electrode, and a saturated calomel electrode (SCE) as a reference electrode. The working electrode was prepared by coating the ethanol suspension of the sample onto a clean indium tin oxide (ITO) glass and was dried in vacuum at 70 °C. The electrodes were immersed in a supporting electrolyte solution of 0.5 M Na_2SO_4 containing 10 vol% lactic acid. Prior to the measurement, the solution was deaerated by bubbling Ar for 1 hour. The working electrode was irradiated with a GY-10 xenon lamp (150W) during the measurement. For the Mott-Schottky measurements, the supporting solution was 0.5 M Na_2SO_4 without adding lactic acid.

2.4 Photocatalytic reaction for hydrogen evolution

The photocatalytic reaction was carried out in a 70 mL quartz flask equipped with a flat optical entry window. The effective irradiation area for the cell is ca. 3 cm^2. In a typical photocatalytic experiment, 60 mL of 10 vol% lactic acid aqueous solution containing 50 mg of the fresh prepared catalyst were added into the quartz flask. Prior to irradiation, the system was sonicated for 3 min at room temperature. The system was deaerated by bubbling argon into the solution for 30 min before light irradiating. A 150 W Xe lamp equipped with a cut-off filter at 420 nm was used as a visible-light source. The lamp was positioned ca. 10 cm away from the optical entry window of the reactor. The produced hydrogen gas was analyzed with an online gas chromatograph (GC1650) equipped with a thermal conductivity detector (TCD) and 5 A molecular sieve columns using argon as carrier gas. The standard H_2/Ar gas mixtures of known concentrations were used for GC signal calibration.

3. Results and discussion

3.1 Characterization of the photocatalysts

The XRD patterns of as-prepared samples are displayed in Fig. 1. The diffraction peaks at 26.5°, 43.8°, and 52.0° (Fig. 1, curve a) correspond to (111), (220), and (311) planes of the cubic structure of CdS (JCPDS card no. 10-0454); while the diffraction peaks at 28.6°, 48.6°, and 56.5° (Fig. 1, curve b) correspond to (111), (220), and (311) planes of the cubic structure of ZnS (JCPDS card no. 05-0566). The formation of $Zn_xCd_{1-x}S$ solid solution is confirmed by the diffraction peaks of CdS shifting to a higher degree (Fig. 1, curve c-f) as the molar ratio of Zn^{2+} to Cd^{2+} increased from 0.1 to 0.4. At higher molar ratio of Zn^{2+} to Cd^{2+} (e.g. n_{Cd}/n_{Zn}=0.5:0.5), ZnS appears as a separate phase in the sample (Fig. 1, curve g). For the MoS_2 modified sample, $Zn_{0.3}Cd_{0.7}S/MoS_2$-0.6, all diffraction peaks locate at ca. 27.0°, 44.8°, and 52.9° (Fig. 1 curve h), which are similar to the pristine $Zn_{0.3}Cd_{0.7}S$ and there were no diffraction peaks attributable to MoS_2, which might be due to the low content and high distribution of the MoS_2 component.

Fig. 2 depicts the XPS spectra of the sample $Zn_{0.3}Cd_{0.7}S/MoS_2$-0.6. The binding energies obtained were corrected for specimen charging by referencing carbon 1s to 284.5 eV. The survey XPS is shown in Fig. 2A. The peaks centred at 411.6 eV and 404.7 eV are attributed to Cd and the peaks at 1024.2 eV and 1047.7 eV are attributed to Zn.[44-45] The high-resolution XPS spectrum of Mo 3d (Fig. 2B) shows binding energy at 228.9 eV for Mo^{4+} $3d_{5/2}$ and 232.1 eV for Mo^{4+} $3d_{3/2}$, suggesting that Mo exist in the chemical states of Mo^{4+}. These values are close to those previously reported for MoS_2.[46] In addition, as compared to the binding energy of Zn 2p reported for $Zn_xCd_{1-x}S$,[44-45] a higher binding energy shift was observed over the sample $Zn_{0.3}Cd_{0.7}S/MoS_2$-0.6. Such a shift to high binding energy may suggest an interaction between $Zn_{0.3}Cd_{0.7}S$ and MoS_2.[47]

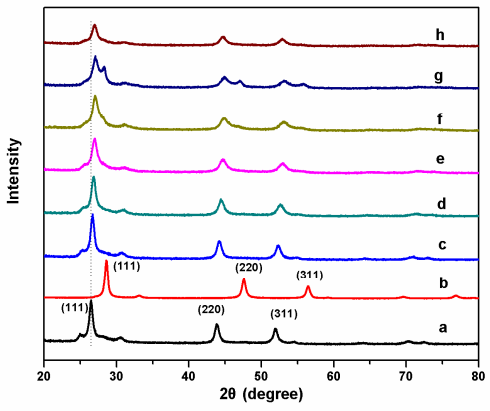

Fig.1 XRD patterns of as-prepared $Zn_xCd_{1-x}S$ samples using the precipitate-hydrothermal method. Sample (a) CdS, (b) ZnS, (c) $Zn_{0.1}Cd_{0.9}S$, (d) $Zn_{0.2}Cd_{0.8}S$, (e) $Zn_{0.3}Cd_{0.7}S$, (f) $Zn_{0.4}Cd_{0.6}S$, (g) $Zn_{0.5}Cd_{0.5}S$, and (h) $Zn_{0.3}Cd_{0.7}S/MoS_2$-0.6.

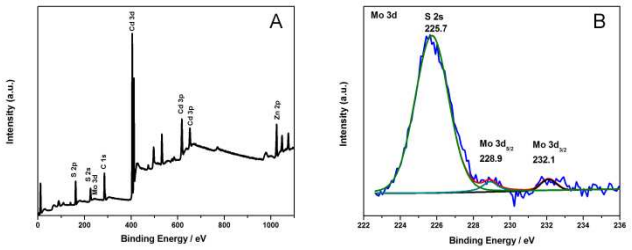

Fig.2 XPS spectra of sample $Zn_{0.3}Cd_{0.7}S/MoS_2$-0.6: (A) the survey spectrum and (B) High-resolution XPS spectrum of Mo 3d.

Fig. 3 shows TEM images of MoS_2 and $Zn_{0.3}Cd_{0.7}S/MoS_2$-0.6. The image of exfoliated MoS_2 (Fig. 3A) shows that crumpled graphene-like molybdenum disulfide is obtained. After the ultrasonic treatment of the mixture of $Zn_{0.3}Cd_{0.7}S$ and graphene-like MoS_2, the $Zn_{0.3}Cd_{0.7}S$ nanoparticles were deposited onto the MoS_2 sheets as shown in Fig. 3B. The particle size of $Zn_{0.3}Cd_{0.7}S$ is about 15±3 nm. The HRTEM image of $Zn_{0.3}Cd_{0.7}S/MoS_2$-0.6 (Fig. 3C) exhibits fringes with the lattice spacing of ca. 0.32 nm and 0.62 nm, which correspond to the (101) plane of cubic $Zn_{0.3}Cd_{0.7}S$ and the (002) plane of hexagonal MoS_2, respectively, indicating the two components coexist in the nanocomposite.

3.2 Optical and photoelectrochemical properties

Fig. 4A shows the UV-vis DRS spectra of the $Zn_xCd_{1-x}S$ samples. Intense absorption bands with the absorption edges in the visible region are observed for all $Zn_xCd_{1-x}S$ samples. The absorption edge shows a continuous blue shift as the Zn content in the $Zn_xCd_{1-x}S$ solid solution increases, indicating that the band gap becomes wider due to the increase of Zn concentration. However, the absorption edge of $Zn_{0.5}Cd_{0.5}S$ shows a little red shift compared to that of the $Zn_{0.4}Cd_{0.6}S$ sample. By the XRD results above, the $Zn_{0.5}Cd_{0.5}S$ sample consists of both $Zn_xCd_{1-x}S$ solid solution and ZnS phase. This may be the reason for the discontinuous blue shift of the $Zn_{0.5}Cd_{0.5}S$ sample. The colour of the $Zn_xCd_{1-x}S$ samples changes from orange to yellow as the Zn content in the solid solution increases (Fig. 4B). Fig. 4C shows the UV-vis DRS spectra of the $Zn_{0.3}Cd_{0.7}S$ and $Zn_{0.3}Cd_{0.7}S/MoS_2$-0.6. The spectra of ZnS, CdS and physical mixture of ZnS and CdS are also demonstrated for comparison. From Fig. 4C we can see that the absorption edge of $Zn_{0.3}Cd_{0.7}S$ lies between that of ZnS (curve a) and CdS (curve b). In addition, the absorption edge of $Zn_{0.3}Cd_{0.7}S$ (curve c) is smooth, indicating that a real solid solution formed. The absorption of the physical mixture of ZnS and CdS in a molar ratio of 3/7 can be resolved into two segments (curve e): the absorption in the UV range of ZnS, and the absorption in the visible region of CdS. Similar absorption feature about mixed semiconductors was also reported.[48] These results clearly indicate that homogeneous $Zn_xCd_{1-x}S$ solid solution is successfully prepared when x is less than 0.3. It has been reported that MoS_2 has a small band gap of around 1.23 eV,[49] corresponding to the absorption in the infrared range. However, the absorption spectrum of the $Zn_{0.3}Cd_{0.7}S/MoS_2$-0.6 sample (curve d) demonstrated obviously red shift and a tail-up phenomenon compared with that of $Zn_{0.3}Cd_{0.7}S$, showing an interaction between $Zn_{0.3}Cd_{0.7}S$ and exfoliated MoS_2 sheets. The extrapolation of the Tauc plot on *x* intercepts gives the band gaps of 2.28, 2.38 and 2.40 eV for $Zn_{0.1}Cd_{0.9}S$, $Zn_{0.2}Cd_{0.8}S$ and $Zn_{0.3}Cd_{0.7}S$, respectively (insets of Fig. 4).

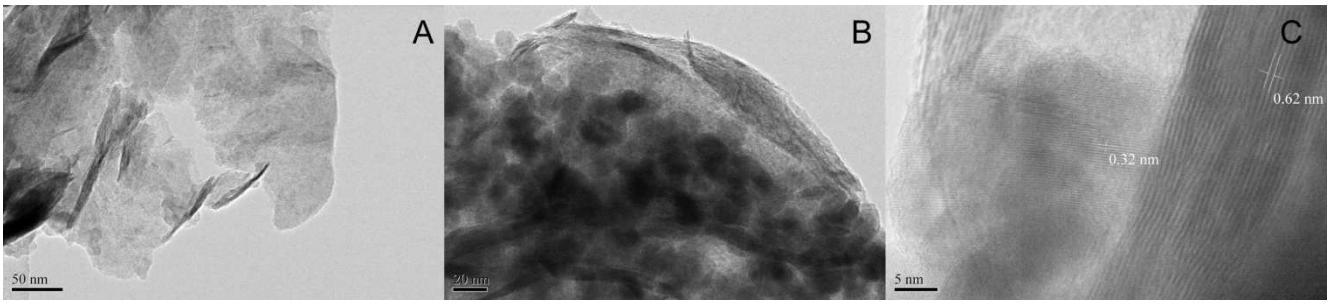

Fig.3 The TEM image of exfoliated MoS_2 (A) and HRTEM images of $Zn_{0.3}Cd_{0.7}S/MoS_2$-0.6 photocatalyst (B) and (C).

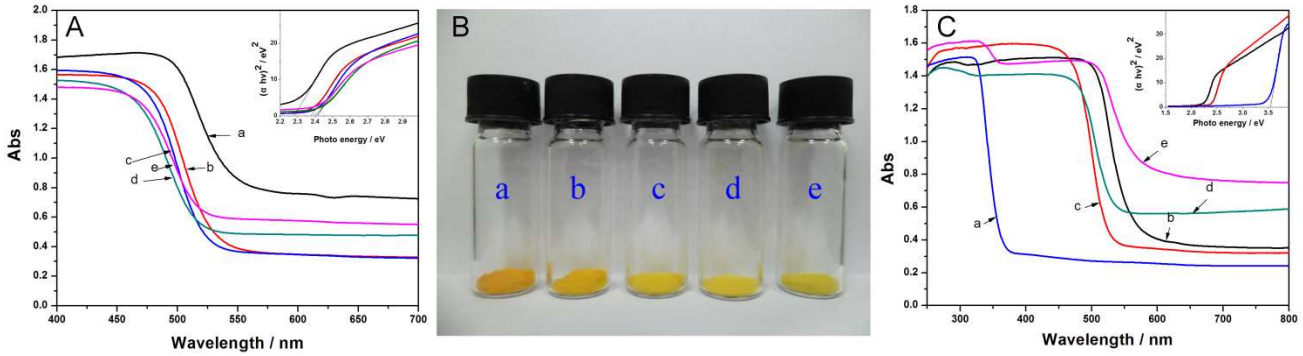

Fig.4 A: UV–vis diffuse reflectance spectra and the band gap calculation of the samples (a) $Zn_{0.1}Cd_{0.9}S$, (b) $Zn_{0.2}Cd_{0.8}S$, (c) $Zn_{0.3}Cd_{0.7}S$, (d) $Zn_{0.4}Cd_{0.6}S$, (e) $Zn_{0.5}Cd_{0.5}S$. B : The photo images of the (a) $Zn_{0.1}Cd_{0.9}S$, (b) $Zn_{0.2}Cd_{0.8}S$, (c) $Zn_{0.3}Cd_{0.7}S$, (d) $Zn_{0.4}Cd_{0.6}S$, (e) $Zn_{0.5}Cd_{0.5}S$ C: UV–Vis diffuse reflectance spectra and the band gap calculation of the samples (a) ZnS, (b) CdS, (c) $Zn_{0.3}Cd_{0.7}S$, (d) $Zn_{0.3}Cd_{0.7}S/MoS_2$-0.6, (e) physical mixture of ZnS and CdS (mole ratio: 3:7). The band gap value of samples estimated by a related curve of $(\alpha h\nu)^2$ versus photon energy plotted in the inset.

Cite this: DOI: 10.1039/c0xx00000x

www.rsc.org/xxxxxx

ARTICLE TYPE

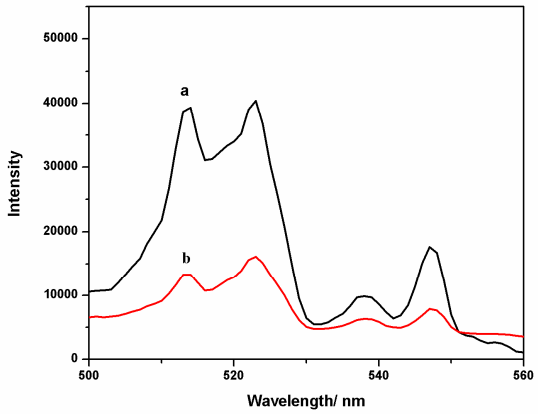

Fig.5 Fluorescence spectra of (a) $Zn_{0.3}Cd_{0.7}S$ sample and (b) $Zn_{0.3}Cd_{0.7}S/MoS_2$-0.6 sample. Excited wavelength: 466 nm.

The photoluminescence spectra (PL) of the as-prepared samples are measured to reveal the photogenerated charge transfer process. As shown in Fig. 5, four emission peaks at 514 nm, 523 nm, 537 nm, and 547 nm can be observed for both $Zn_{0.3}Cd_{0.7}S$ and $Zn_{0.3}Cd_{0.7}S/MoS_2$-0.6 at 466 nm excitation. The peaks at 514 nm and 523 nm correspond to the near-band emission of the zinc cadmium sulphide while the peaks at 537 nm and 547 nm commonly arise from the deep-level or trap-state emission of the zinc cadmium sulphide.[50] From Fig. 5, the PL intensity of $Zn_{0.3}Cd_{0.7}S/MoS_2$-0.6 decreased greatly compared with that of $Zn_{0.3}Cd_{0.7}S$. The calculated quenching efficiency at 514 nm for $Zn_{0.3}Cd_{0.7}S/MoS_2$-0.6 is 66.9%.[51] This phenomenon is attributed to the efficient electron transfer from the $Zn_{0.3}Cd_{0.7}S$ to the graphene-like MoS_2 sheets, leading to the spatial separation of the photogenerated electron and the hole.[52-54]

The photocurrent-time experiments were conducted to investigate the photo-excited electron transfer in the as-prepared samples and the results are shown in Fig. 6A. Under UV-vis illumination, the photocurrent response of the $Zn_{0.3}Cd_{0.7}S$ electrode was strong but not very steady. The average photocurrent density is ca. 340 μA cm^{-2} for the five light-on and light-off cycles. An enhanced photocurrent response for $Zn_{0.3}Cd_{0.7}S/MoS_2$-0.6 electrode was observed under the similar experimental conditions and the photocurrent density reaches ca. 440 μA cm^{-2}. The photocurrent response for the $Zn_{0.3}Cd_{0.7}S/MoS_2$-0.6 electrode was prompt, steady, and reproducible during the light on/off illumination cycles. The enhancement and the stability of the photocurrent for the $Zn_{0.3}Cd_{0.7}S/MoS_2$-0.6 sample are owing to positive synergetic effect between $Zn_{0.3}Cd_{0.7}S$ and MoS_2 in the nanocomposite. Graphene-like MoS_2 in the nanocomposite may serve as an acceptor and a transporter for the excited electrons generated from $Zn_{0.3}Cd_{0.7}S$, thus, promotes the photoexcited e^-/h^+ pair separation and enhances the charge transfer from the nanocomposite to ITO.

The results of the liner sweep voltammetry of $Zn_{0.3}Cd_{0.7}S$ and $Zn_{0.3}Cd_{0.7}S/MoS_2$-0.6 electrodes are shown in Fig. 6B. For $Zn_{0.3}Cd_{0.7}S$ electrode, the proton reduction potential is ca. -1.09 V vs. SCE; while for $Zn_{0.3}Cd_{0.7}S/MoS_2$-0.6 electrode, the value changes to -1.03 V vs. SCE.[55] The result demonstrates that the introduction of graphene-like MoS_2 sheet in the composite reduces the hydrogen evolution potential.

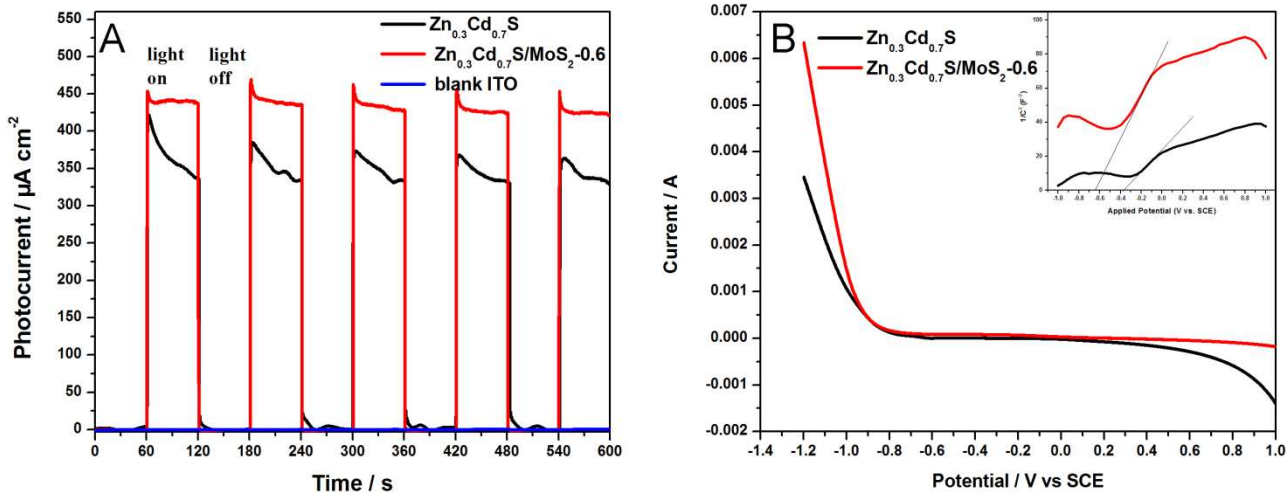

Fig.6 (A) Transient photocurrent-time curves of blank ITO glass (blue line), $Zn_{0.3}Cd_{0.7}S$ (black line) and $Zn_{0.3}Cd_{0.7}S/MoS_2$-0.6 (red line) in Na_2SO_4 solution(0.50 M) containing 10% volume lactic acid under visible-light irradiation in Ar. Initial voltage: 0.1 V; (B) The liner sweep voltammetry of $Zn_{0.3}Cd_{0.7}S$ and $Zn_{0.3}Cd_{0.7}S/MoS_2$-0.6 electrodes in 0.50 mol/L Na_2SO_4 (10 vol% lactic acid). Hydrogen evolution potentials at 0.002 A were as follows: $Zn_{0.3}Cd_{0.7}S$, E=-1.09 V; $Zn_{0.3}Cd_{0.7}S/MoS_2$, E=-1.03 V. Inset: Mott-Schottky plot of the $Zn_{0.3}Cd_{0.7}S$ and $Zn_{0.3}Cd_{0.7}S/MoS_2$-0.6 sample.

Cite this: DOI: 10.1039/c0xx00000x

www.rsc.org/xxxxxx

ARTICLE TYPE

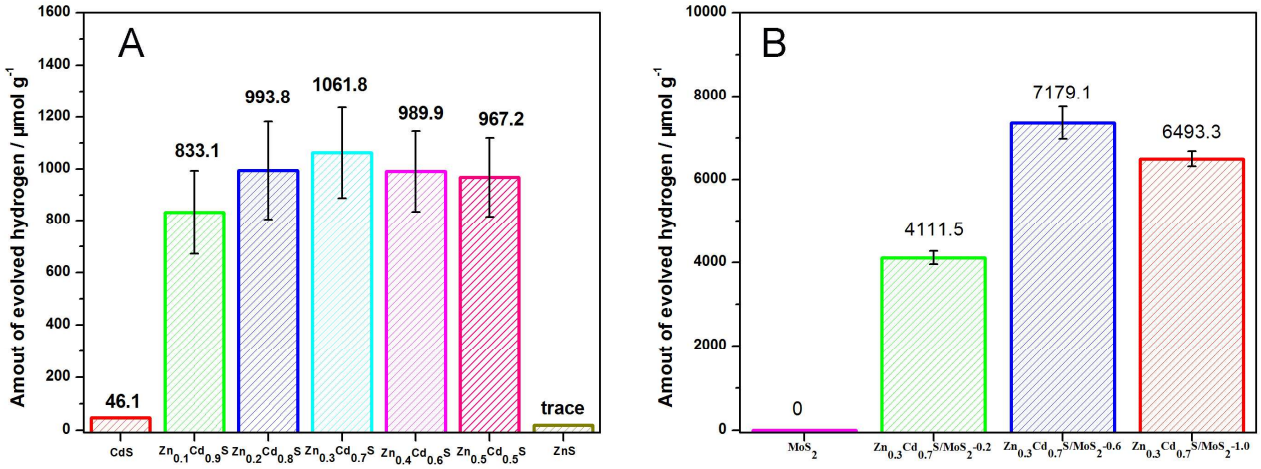

Fig.7 The hydrogen production of the solid solution of $Zn_xCd_{1-x}S$ samples (A) and $Zn_{0.3}Cd_{0.7}S/MoS_2$ samples (B) in 6 hours. Reaction conditions: 50 mg photocatalyst, 6 mL lactic acid, 54 mL deionized water, 150 W Xe lamp equipped with a cut-off filter at 420 nm.

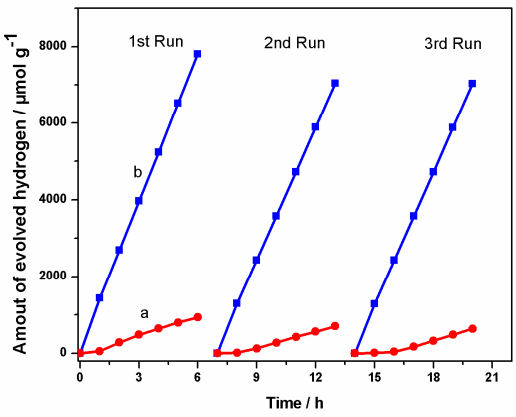

Fig.8 The recycling experiment of the $Zn_{0.3}Cd_{0.7}S$ (a) and $Zn_{0.3}Cd_{0.7}S/MoS_2$-0.6 (b). Reaction conditions: 50 mg photocatalyst, 6 mL lactic acid, 54 mL deionized water, 150 W Xe lamp equipped with a cut-off filter at 420 nm

In order to further understand the function of graphene-like MoS_2 sheet in the nanocomposite, we measured flat band potentials of $Zn_{0.3}Cd_{0.7}S$ and $Zn_{0.3}Cd_{0.7}S/MoS_2$-0.6. The flat band potential (E_{fb}) was determined by the onset potential of the Mott–Schottky plots[56] and the results are shown in the inset of Fig. 6B. The positive slopes of the linear plot suggest n-type semiconductor features of $Zn_{0.3}Cd_{0.7}S$ and $Zn_{0.3}Cd_{0.7}S/MoS_2$-0.6.[57] E_{fb} of $Zn_{0.3}Cd_{0.7}S$ estimated from the *x* intercepts of the linear region of the Mott–Schottky plot is ca. −0.4 V vs. SCE; while ca. −0.7 V vs. SCE for $Zn_{0.3}Cd_{0.7}S/MoS_2$-0.6 electrode. These results shows $Zn_{0.3}Cd_{0.7}S/MoS_2$-0.6 possesses a higher electron donor level than $Zn_{0.3}Cd_{0.7}S$, suggesting coupling $Zn_{0.3}Cd_{0.7}S$ and graphene-like MoS_2 may produce a positive synergetic effect to shift the flat potential of the nanocomposite to a more negative position. This negative shift is certainly beneficial for the photocatalytic hydrogen evolution.

3.3 Photoinduced hydrogen evolution

The photocatalytic performance for hydrogen production over $Zn_xCd_{1-x}S$ catalysts under visible-light irradiation (λ>420 nm) is shown in Fig. 7A. The amount of hydrogen evolved from pure CdS is low (46.1 μmol g^{-1}) due to its large H_2 evolution overpotential and the absence of the cocatalyst.[58-60] Only trace amount of hydrogen can be detected from pure ZnS because it can't absorb visible-light. However, the $Zn_xCd_{1-x}S$ solid solution catalyst demonstrated very nice photocatalytic performance for hydrogen production under visible-light irradiation. The total amount of hydrogen evolved over $Zn_{0.1}Cd_{0.9}S$ is 833.1 μmol g^{-1} under visible-light irradiation. The evident enhancement of the H_2 production from $Zn_{0.1}Cd_{0.9}S$ owns to the suitable band gap and position of the $Zn_{0.1}Cd_{0.9}S$ solid solution for the visible-light-driven photocatalytic hydrogen production from water.[1] Since both the band gap and position can be adjusted by varying the ratio of the compositions of the narrow and the wide band gap semiconductor in the solid solution, the optimized solid solution used as the photocatalyst was found to be $Zn_{0.3}Cd_{0.7}S$ and the H_2 generation rate under visible-light irradiation reached 1061.8 μmol g^{-1}. However, the photocatalytic activity decreased with increasing ZnS content in the solid solution.

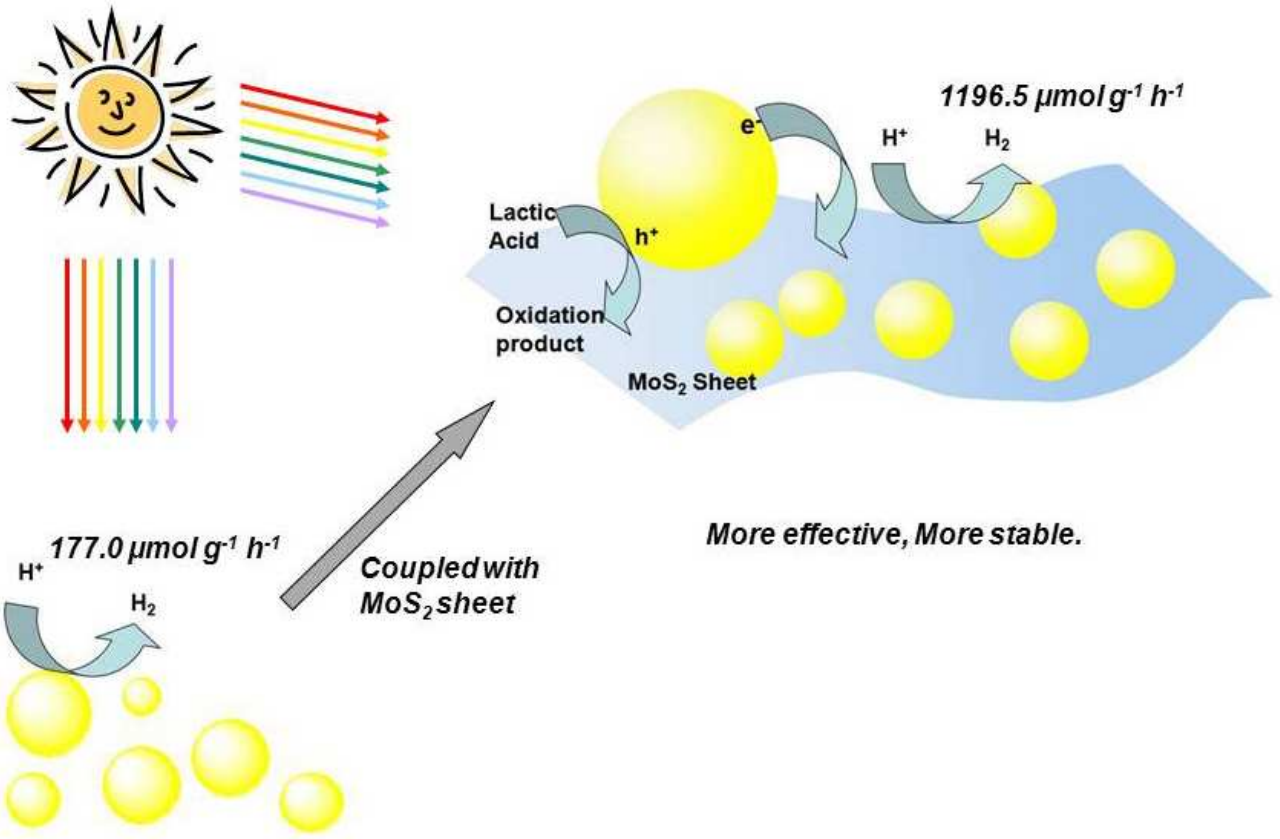

Fig.9 Schematic illustration for the visible-light photocatalytic performance of the $Zn_{0.3}Cd_{0.7}S$ and $Zn_{0.3}Cd_{0.7}S/MoS_2$ nanostructures

Fig. 7B shows the photocatalytic activity of $Zn_{0.3}Cd_{0.7}S/MoS_2$ photocatalysts with different amounts of MoS_2 in the nanocomposite. No H_2 was detected when MoS_2 was used as the photocatalyst, suggesting that MoS_2 itself was not active for photocatalytic H_2 evolution. Introduction of MoS_2 in the composite leads to a huge hydrogen production enhancement. Under visible-light irradiation, the total amount of hydrogen evolved over $Zn_{0.3}Cd_{0.7}S/MoS_2$-0.2 and $Zn_{0.3}Cd_{0.7}S/MoS_2$-0.6 were 4111.5 μmol g^{-1} and 7179.1 μmol g^{-1}, which is ca. 4 times and 7 times as high as that of $Zn_{0.3}Cd_{0.7}S$ respectively. The amount of H_2 evolved starts to decrease when the content of MoS_2 in the nanocomposite was above the optimized value, which is ~0.6 wt%. Since the MoS_2 itself was inactive for photocatalytic hydrogen evolution, excessive amount of MoS_2 in the nanocomposite may block the light-absorption and weaken the light intensity arriving at the surface of $Zn_{0.3}Cd_{0.7}S$, thus decreases the photocatalytic activity.

Owing to the importance of the stability of a photocatalyst for its practical application, the photocatalytic stability of $Zn_{0.3}Cd_{0.7}S/MoS_2$-0.6 was further investigated by cycle photocatalytic experiments and the results are shown in Fig. 8. For comparison, the photocatalytic stability of $Zn_{0.3}Cd_{0.7}S$ was also investigated in the same conditions. Under 6 h visible-light irradiation, $Zn_{0.3}Cd_{0.7}S$ produced ca. 937.8 μmol g^{-1} H_2 in the first run, and 706.2 μmol g^{-1} H_2 in the second run. In the third run, the amount of evolved hydrogen decreased to 637.8 μmol g^{-1}. While $Zn_{0.3}Cd_{0.7}S/MoS_2$-0.6 in the first run produces ca. 7806.0 μmol g^{-1} hydrogen under visible-light irradiation. In the second run, the photocatalytic activity of $Zn_{0.3}Cd_{0.7}S/MoS_2$-0.6 decreased ca. ten percent (7039.8 μmol g^{-1}). However, the amount H_2 evolved in the third run (7030.2 μmol g^{-1}) is almost the same as that of the second run. The results suggest that $Zn_{0.3}Cd_{0.7}S/MoS_2$-0.6 is much more stable than $Zn_{0.3}Cd_{0.7}S$ under visible-light irradiation.

On the basis of above results, a possible mechanism for visible-light induced hydrogen production on the $Zn_{0.3}Cd_{0.7}S/MoS_2$ nanocomposite is shown in Fig. 9. Under visible-light irradiation, the electrons in the valence band of $Zn_{0.3}Cd_{0.7}S$ are excited to the conduction band. Then, the excited electrons transfer from the conduction band of $Zn_{0.3}Cd_{0.7}S$ to the MoS_2 nanosheets because of the low Fermi energy level of MoS_2 (ca. -0.1 eV) and the superior interfacial contacts between $Zn_{0.3}Cd_{0.7}S$ and MoS_2, which enhances the charge separation and suppresses the recombination of e^-/h^+ pairs. H^+ ions in the solution accept the electrons from MoS_2 and forms H_2. Graphene-like MoS_2 here also acts as hydrogen evolution centres and reduces hydrogen evolution overpotential greatly. The holes remained on the surface of $Zn_{0.3}Cd_{0.7}S$ nanoparticles are consumed by the lactic acid in the solution.

Conclusions

A novel nanocomposite composed of graphene-like MoS_2 and $Zn_xCd_{1-x}S$ solid solution as a photocatalyst has been synthesized. $Zn_xCd_{1-x}S$ nanoparticles well anchored on the two-dimensional graphene-like MoS_2 sheets of the nanocomposite, resulting in the excellent interfacial contacts between $Zn_xCd_{1-x}S$ and graphene-like MoS_2. Graphene-like MoS_2 in the nanocomposite serves not only as an excellent supporting matrix for anchoring $Zn_xCd_{1-x}S$ nanoparticles but also as a superior electron mediator to adjust electron transfer, and as the hydrogen evolution centres. It efficiently promotes the electron-hole separation, lengthens the charge lifetimes in the process of photocatalytic reaction, and reduces hydrogen evolution overpotential. The photocatalyst with the optimal composition showed much higher photocatalytic performance and superior stability for H_2 evolution under visible-light irradiation. This study demonstrates an efficient method to construct a low-cost but effective photocatalyst for water splitting to produce hydrogen under solar light irradiation.

Acknowledgements

The authors are grateful for the financial support of this research by the National Natural Science Foundation of China (21373143 and 51273141), the Priority Academic Program Development of Jiangsu Higher Education Institutions (PAPD) and Grand Challenge Canada-Rising Star Program (GCC-CRC3 0099-01).

Notes and references

[a] *College of Chemistry, Chemical Engineering and Materials Science, Soochow University, Suzhou, 215123, China. E-mail: pyang@suda.edu.cn; Fax: +86 512-65880089; Tel: +86 512-65880089*
[b] *Department of Chemistry and Physics, University of Toronto, Toronto M5S 3H6, Canada Tel/Fax: 1-416-978-4526; E-mail: clu@chem.utoronto.ca.*

1 X. B. Chen, S. H. Shen, L. J. Guo. Samuel S. Mao, *Chem. Rev.*, 2010, **110**, 6503-6570.
2 K. Zhang and L. J. Guo, *Catal. Sci. Technol.*, 2013, **3**, 1672-1690.
3 H. L. Zhou, Y. Q. Qu, Tahani Zeid and X. F. Duan, *Energy. Environ. Sci.*, 2012, **5**, 6732-6743.
4 A. Fujishima and K. Honda, *Nature*, 1972, **238**, 37-38.
5 Jean-Franqois Reber and Milös Rusek. *J. Phys. Chem.* 1986, **90**, 824-834.
6 Z. Khan, M Khannam, N. Vinothkumar, M. Deb and M. Qureshi, *J. Mater. Chem.*, 2012, **22**, 12090-12095.
7 X. Zong, H. J. Yan, G.P. Wu, G. J. Ma, F. Y. Wen, L. Wang, C. Li, *J. Am. Chem. Soc.*, 2008, **130**, 7176-7177.
8 Z. Khan, M. Khannam, M. Qureshi, N. V. Kumar, M. De, *J. Mater. Chem. A*, 2012, **22**, 12090–12095.
9 A. Deshpande, N. M. Gupta. *Int J Hydrogen Energy,* 2010, **35**, 3287-3296.
10 X.C. Wang, K. Maeda, A. Thomas, K. Takanabe, G. Xin, J.M. Carlsson, K. Domen, M. Antonietti, *Nat. Mater.*, 2009, **8**, 76-80.
11 Y. Wang, J. Hong, W. Zhang and R. Xu, *Catal. Sci. Technol.*, 2013, **3**, 1703-1711.
12 H. J. Yan, Y. Chen, S. M. Xu, *Int. J. Hydrogen Energy*, 2012, **37**, 125-133.
13 G. G. Zhang, J. S. Zhang, M. W. Zhang, X. C. Wang, *J. Mater. Chem.*, 2012, **22**, 8083-8091.
14 J. D. Hong, X. Y. Xia, Y. S. Wang, and R. Xu, *J. Mater. Chem.*, 2012, **22**, 15006-15012.
15 K. Maeda, H. Terashima, K. Kase, K. Domen. *Catal. Sci. Technol.*, 2012, **2**, 818-823.
16 K. Maeda, H. Terashima, K. Kase, K. Domen. *Appl. Catal. A*, 2009, **357**, 206-212.
17 K. Zhang, D. W. Jing, C. J. Xing, L. J. Guo, *Int. J. Hydrogen Energy*, 2007, **32**, 4685-4691.
18 W. Zhang, R. Xu, *Int. J. Hydrogen Energy*, 2009, **34**, 8495-8503.
19 L. Wang, W. Z. Wang, M. Shang, W. Z. Yin, S. M. Sun, L. Zhang, *Int. J. Hydrogen Energy*, 2010, **35**, 19-25.
20 Z. B. Yu, Y. P. Xie, G. Liu, G. Q. Lu, X. L. Ma and H. M. Cheng, *J. Mater. Chem. A*, 2013, **1**, 2773-2776.
21 Q. Li, B. D. Guo, J. G. Yu, J. R. Ran, B. H. Zhang, H. J. Yan, J. R. Gong. *J. Am. Chem. Soc.*, 2011, **133**, 10878-10884.
22 A. Suryawanshi, P. Dhanasekaran, D. Mhamane. S.Kelkar, S. Patil, N. Gupta, S. Ogale. *Int. J. Hydrogen Energy*, 2012, **37**, 9584-9589.
23 Q. J. Xiang, J. G. Yu, M. Jaroniec, *J, Phys, Chem, C*, 2011, **115**, 7355-7363.
24 Z. G. Mou, S. L. Yin, M. S. Zhu, Y. K. Du, X. M. Wang, P. Yang, J. W. Zheng and C. Lu, *Phys. Chem. Chem. Phys.*, 2013, **15**, 2793-2799.
25 K. Takanabe, K. Kamata, X. C. Wang, M. Antonietti, J. Kubota, K. Domen. *Phys. Chem. Chem. Phys.*, 2010, **12**, 13020-13025.
26 S. X. Min, G. X. Lu. *J. Phys. Chem. C*, 2012, **116**, 19644-19652.
27 N. Z. Bao, L. M. Shen, T. Takata, K. Domen. *Chem. Mater.*, 2008, **20**, 110-117.
28 P. S. Lunawat, R. Kumar, N. M. Gupta. *Catal. Lett.,* 2008, **121**, 226–233.
29 M. Nguyen, P. D. Tran, S. S. Pramana, R. L. Lee, S. K. Batabyal, N. Mathews, L. H. Wong and M. Graetzel. *Nanoscale,* 2013, **5**, 1479–1482.
30 Jean-Franqois Reber and Kurt Meier. *J. Phys. Chem.*, 1984, **88**, 5903-5913.
31 J. Y. Zhang, Y. H. Wang, J. Zhang, Z. Lin, F. Huang, and J. G. Yu. *ACS Appl. Mater. Interfaces*, 2013, **5**, 1031-1037.
32 Agileo Hernández-Gordillo, Francisco Tzompantzi, Ricardo Gómez. *Int. J. Hydrogen Energy*, 2012, **37**, 17002-17008.
33 M. T. Li, J. G. Jiang, L. J. Guo. *Int. J. Hydrogen Energy*, 2010, **35**, 7036-7042.
34 Y. B. Wang, Y. S. Wang, R. Xu, *Int. J. Hydrogen Energy*, 2010, **35**, 5245-5253.
35 X. H. Zhang, D. W. Jing, L. J. Guo, *Int. J. Hydrogen Energy*, 2010, **35,** 7051-7057.
36 X. Q. An and J. C. Yu., *RSC Adv*, 2011. **1,** 1426-1434.
37 P. V. Kamat. *J. Phys. Chem. Lett,*. 2011, **2,** 242-251.
38 Q. J. Xiang, J. G. Yu and M. Jaroniec. *Chem. Soc. Rev.*, 2012, **41,** 782-796.
39 A. O'Neill, U. Khan and J. N. Coleman, *Chem. Mater.*, 2012, **24,** 2414-2421.
40 X. N. Guo, X. L. Tong, Y. W. Wang, C. M. Chen, G. Q. Jin and X. Y. Guo, *J. Mater. Chem. A*, 2013, **1**, 4657-4661.
41 Q. J. Xiang, J. G. Yu, M. Jaroniec, *J. Am. Chem. Soc.*, 2012, **134**, 6575-6578.
42 X. L. Li and Y. D. Li. *J. Phys. Chem. B*, 2004, **108**, 13893-13900.
43 J. N. Coleman, M. Lotya, A. O'Neill, S. D. Bergin, P. J. King, U. Khan, K. Young, A. Gaucher, S. De, R. J. Smith, I. V. Shvets, S. K. Arora, G. Stanton, H.-Y. Kim, K. Lee, G. T. Kim, G. S. Duesberg, T. Hallam, J. J. Boland, J. J. Wang, J. F. Donegan, J. C. Grunlan, G. Moriarty, A. Shmeliov, R. J. Nicholls, J. M. Perkins, E. M. Grieveson, K. Theuwissen, D. W. McComb, P. D. Nellist and V. Nicolosi, *Science*, 2011, **331**, 568-571.
44 P. K. Narayanam, P, Soni, R. S. Srinivasa, S. S. Talwar, and S. S. Major. *J. Phys. Chem. C,* 2013, **117**, 4314–4325.
45 X. W. Wang, G. Liu, Z. G. Chen, F. Li, L. Z. Wang, G. Q. Lu and H. M. Cheng. *Chem.Comm.*, 2009, **45**, 3452–3454.
46 W. Ho, J. C. Yu, J. Lin, J. G. Yu, and P. S. Li. *Langmuir,* 2004, **20**, 5865-5869.
47 L. Wei, Y J. Chen, Y. P. Lin, H. S. Wu, R. S. Yuan, Z. H. Li. *Appl. Catal. B: Environ.* 2014, **114**, 521– 527.
48 Y. B. Wang, J. C. Wu, J. W. Zheng, R. R. Jiang, R. Xu, *Catal. Sci. Technol.*, 2012, **2**, 581-588.
49 W. Zhou, Z. Yin, Y. Du, X. Huang, Z. Zeng, Z. Fan, H. Liu, J. Wang and H. Zhang, *Small*, 2013, **9**, 140-147.
50 X. B. He and L. Gao. *J. Phys. Chem. C*, 2009, **113**, 10981–10989.
51 L. L. Zhang, Y. T. Lu, Y. K. Du, P. Yang and X. M. Wang, *J. Porphyrins Phthalocyanines,* 2010, **14**, 540–546.

52 M. S. Zhu, Y. T. Lu, Y. K. Du, J. Li, X. M. Wang and P. Yang, *Int. J. Hydrogen Energy*, 2011, **36**, 4298-4304.
53 H. N. Kim, T. W. Kim, I. Y. Kim and S.-J. Hwang. *Adv. Func. Mater.,* 2011, **21**, 3111-3118.
54 M. S. Zhu, Z. Li, B. Xiao, Y. T. Lu, Y. K. Du, P. Yang, and X. M. Wang, *ACS Appl. Mater. Interfaces*, 2013, **5**, 1732−1740.
55 F. A. Frame and F. E. Osterloh, *J. Phys. Chem. C* 2010, **114**, 10628–10633.
56 F. Cardon and W. P. Gomes, *J. Phys. D: Appl. Phys.,* 1978, **11**, L63.
57 R. O'Hayre, M. Nanu, J. Schoonman and A. Goossens, *J. Phys. Chem. C*, 2007, **111**, 4809-4814.
58 Y. X. Li, Y. F. Hu, S. Q. Peng, G. X. Lu, and S. B. Li. *J. Phys. Chem. C,* 2009, **113**, 9352-9358.
59 J. G. Yu, Y. F. Yu, B. Cheng. *RSC Adv*. 2012, **2**, 11829-11835.
60 J. G. Yu, J. Zhang, and M. Jaroniec. *Green Chem.,* 2010, **12**, 1611-1614.